Supplementary information

A. Supplementary results

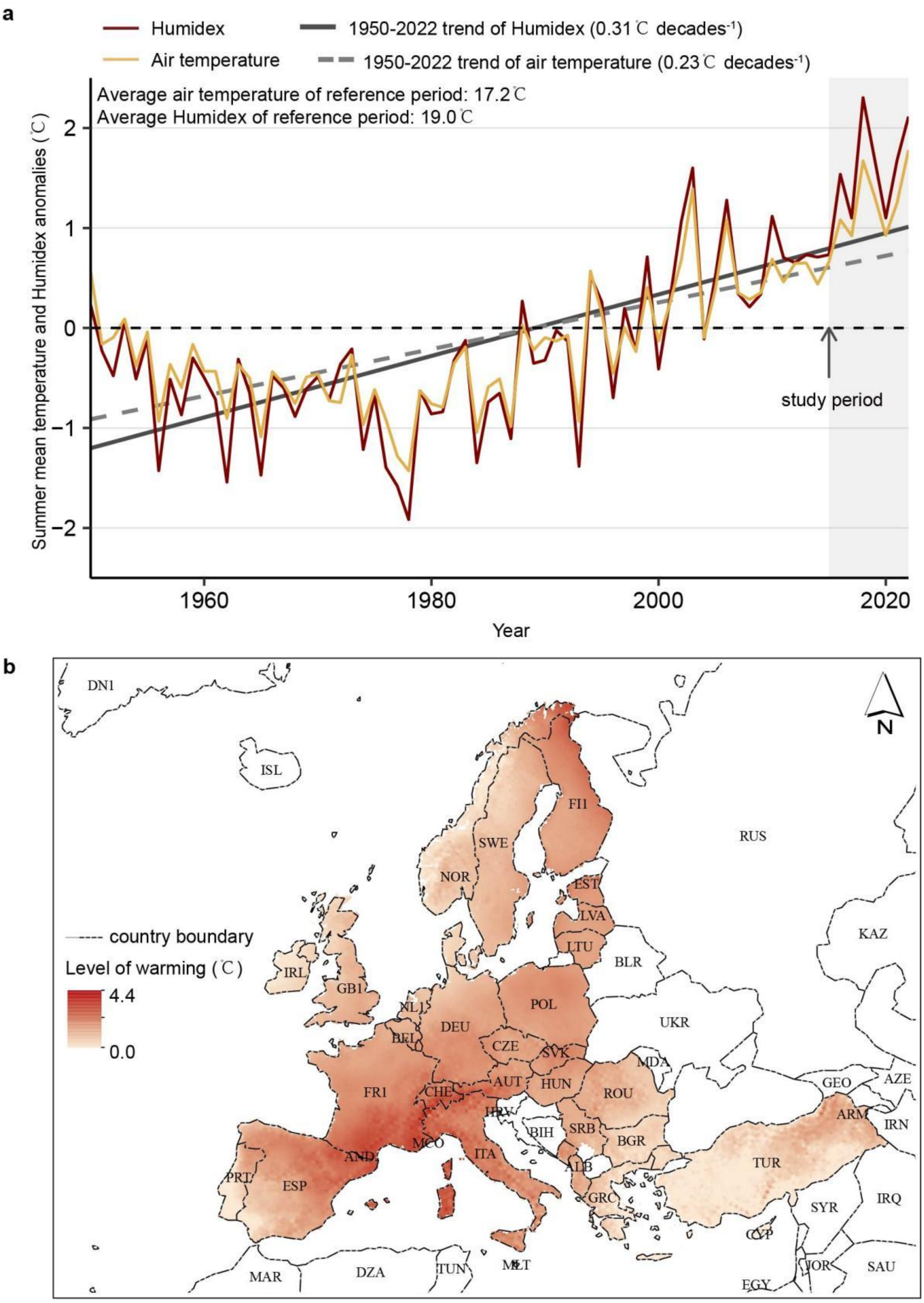

Supplementary Fig 1. Summertime warming in Europe. **(a)** Regional area-weighted mean anomalies (relative to 1986–2005) of Humidex (red) and surface air temperature (orange) in summer (weeks 22-35) over 1950 – 2022. (**b**) The geographic pattern of summertime mean Humidex anomalies (relative to 1986–2005) in 2022. The abbreviations for the European countries are as follows: Finland (FLI), Sweden (SWE), Norway (NOR), Estonia (EST), Latvia (LVA), Lithuania (LTU), United Kingdom (GB1), Ireland (IRL), Netherlands (NL1), Germany (DEU), Belgium (BEL), France (FR1), Poland (POL), Czechia (CZE), Slovakia (SVK), Hungary (HUN), Austria (AUT), Liechtenstein (LIE), Switzerland (CHE), Monaco (MCO), Italy(ITA), Spain (ESP), Portugal (PRT), Romania (ROU), Bulgaria (BGR), Republic of Serbia (SRB), Greece (GRC), Albania (ALB), Turkey (TUR), Cyprus (CYP), and Malta (MLT).

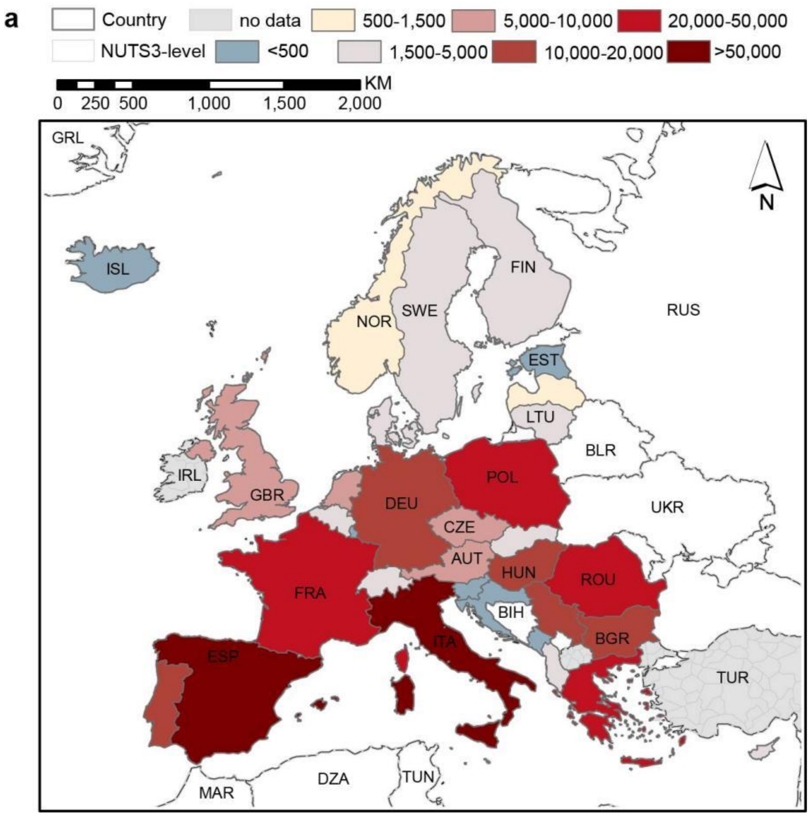

Supplementary Fig 2. Cumulative heat-related deaths in summer (weeks 22-35)

from 2015 to 2022. The abbreviations for the European countries are as follows: Finland (FLI), Sweden (SWE), Norway (NOR), Estonia (EST), Latvia (LVA), Lithuania (LTU), United Kingdom (GB1), Ireland (IRL), Netherlands (NL1), Germany (DEU), Belgium (BEL), France (FR1), Poland (POL), Czechia (CZE), Slovakia (SVK), Hungary (HUN), Austria (AUT), Liechtenstein (LIE), Switzerland (CHE), Monaco (MCO), Italy(ITA), Spain (ESP), Portugal (PRT), Romania (ROU), Bulgaria (BGR), Republic of Serbia (SRB), Greece (GRC), Albania (ALB), Turkey (TUR), Cyprus (CYP), and Malta (MLT).

B. Comparison between air temperature and Humidex in characterizing heat-mortality response

In the comparison of air temperature and Humidex to characterize the relationship between heat exposure and mortality, we found that using the humid heat stress index, Humidex, lead to narrower confidence intervals at the tail of the curve, signifying a greater level of certainty in the illustration of model (Supplementary Fig 3). It reminds us to employ a more accurate characterization of heat impact on human health using Humidex, an integration of air temperature and humidity. Therefore, we chose to use Humidex in our estimation of the heat-mortality curve. This choice was also based on its ability to capture the complex interplay between temperature and humidity, which provides a more robust measure of the potential health effects associated with heat events.

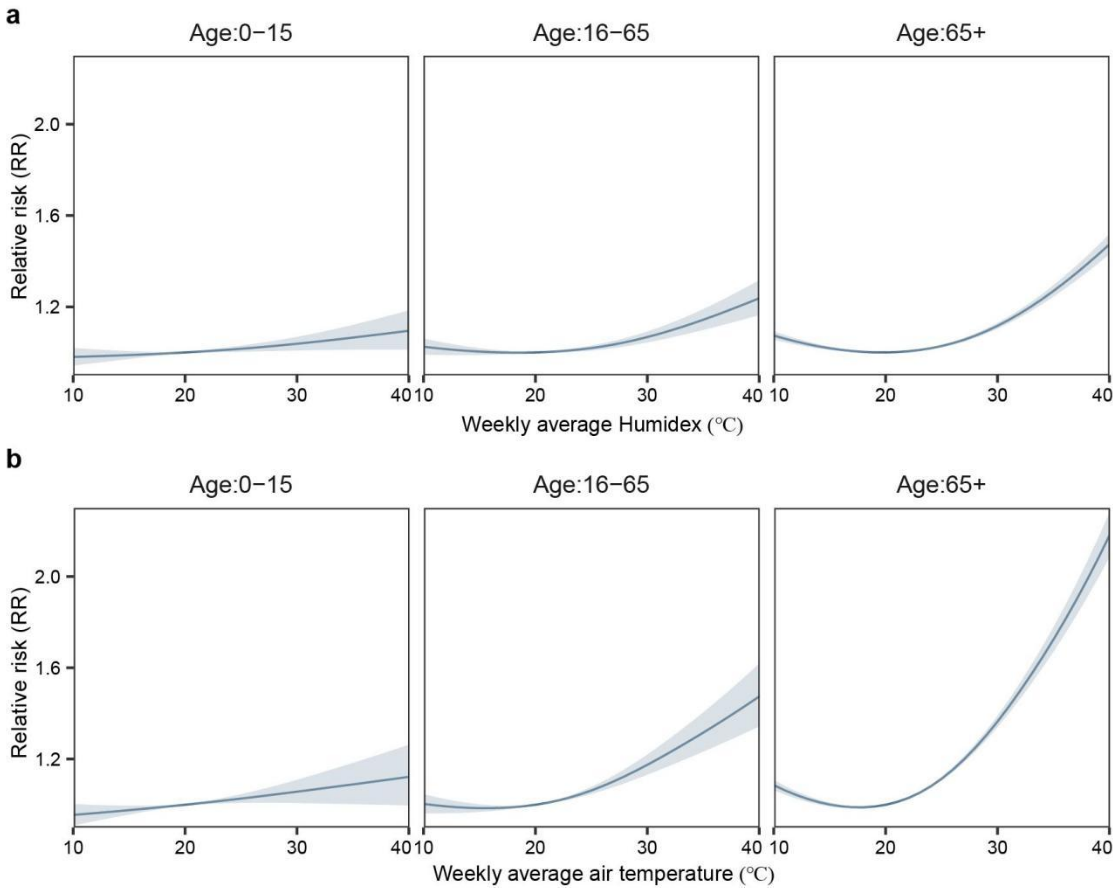

Supplementary Fig 3. Comparison of cumulative relative risk-weekly average heat response curves across three age groups: children (0-15), working-age population (16-65) and elderly population (65+) between Humidex (a) and air temperature (b). The cumulative relative risk of death (unitless) is presented for each age group (blue) and their 95% confidence intervals (95% CI, shaded blue area), calculated versus the minimum mortality Humidex (MMH) of the elderly.

C. Validation

C.1 Humidex data accuracy

We validated our results using hourly in-situ data from NOAA, accessible at [https://www.ncei.noaa.gov/metadata/geoportal/rest/metadata/item/gov.noaa.ncdc:C00

532/html](last assess: October 2023). Four statistical metrics, correlation coefficient (r^2), mean absolute error (MAE), root mean square error (RMSE) and Nash–Sutcliffe efficiency index (NSE) 单击或点击此处输入文字。 were employed for model performance evaluation. Supplementary Fig 4 shows the accuracy scatter plot for observed and estimated Humidex, highlighting strong consistency with a population r^2 of 0.90. The population MAE and RMSE were 2.59°C and 3.39°C, respectively. An NSE of 0.81, less than 1, indicates that the prediction errors are significantly lower than the natural variability of hourly Humidex. These results underscore the robustness of our model in accurately estimating Humidex values and provide confidence in the reliability of our findings.

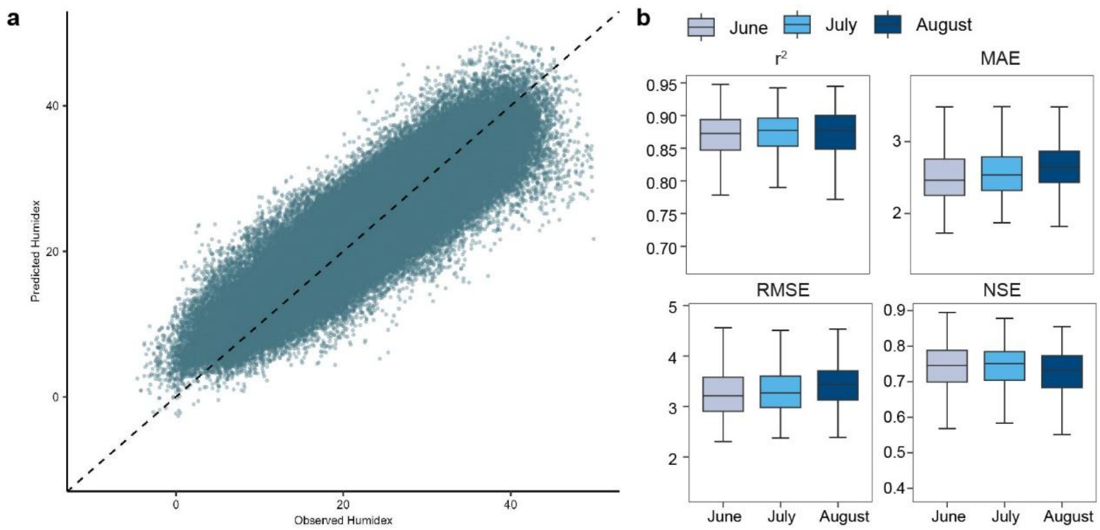

Supplementary Fig 4. Scatter diagrams of the reconstructed humidex model against observed in-situ data (a), and the accuracy validation across month (b).

C.2 Leave-one-out cross validation of DLNM model

The DLNM model was constructed using data from 955 NUTS3-level regions during

2015-2019. To validate the model, we employed a leave-one-out cross validation by splitting the data for each year as an individual test set. The training and validation process was repeated five times in total. The observed number of deaths were compared with the predicted data to indicate the robustness of our model, as shown in Supplementary Fig 5a. The adjusted population R^2 is 0.99 and the population RMSE is 8.81, highlighting the reasonable parameters assumption of our model. Additionally, we assessed the precision of the predictions of each region by comparing the timeline of mortality during June to August for each year. The results revealed a consistent accuracy of the DLNM model unless the selections of training data. Supplementary Fig 5b summarizes the predictive robustness of our model, with R^2 ranging from 0.28 to 0.99 and a mean RMSE of 5.93. This further confirmed the good performance of the DLNM model proposed in our study.

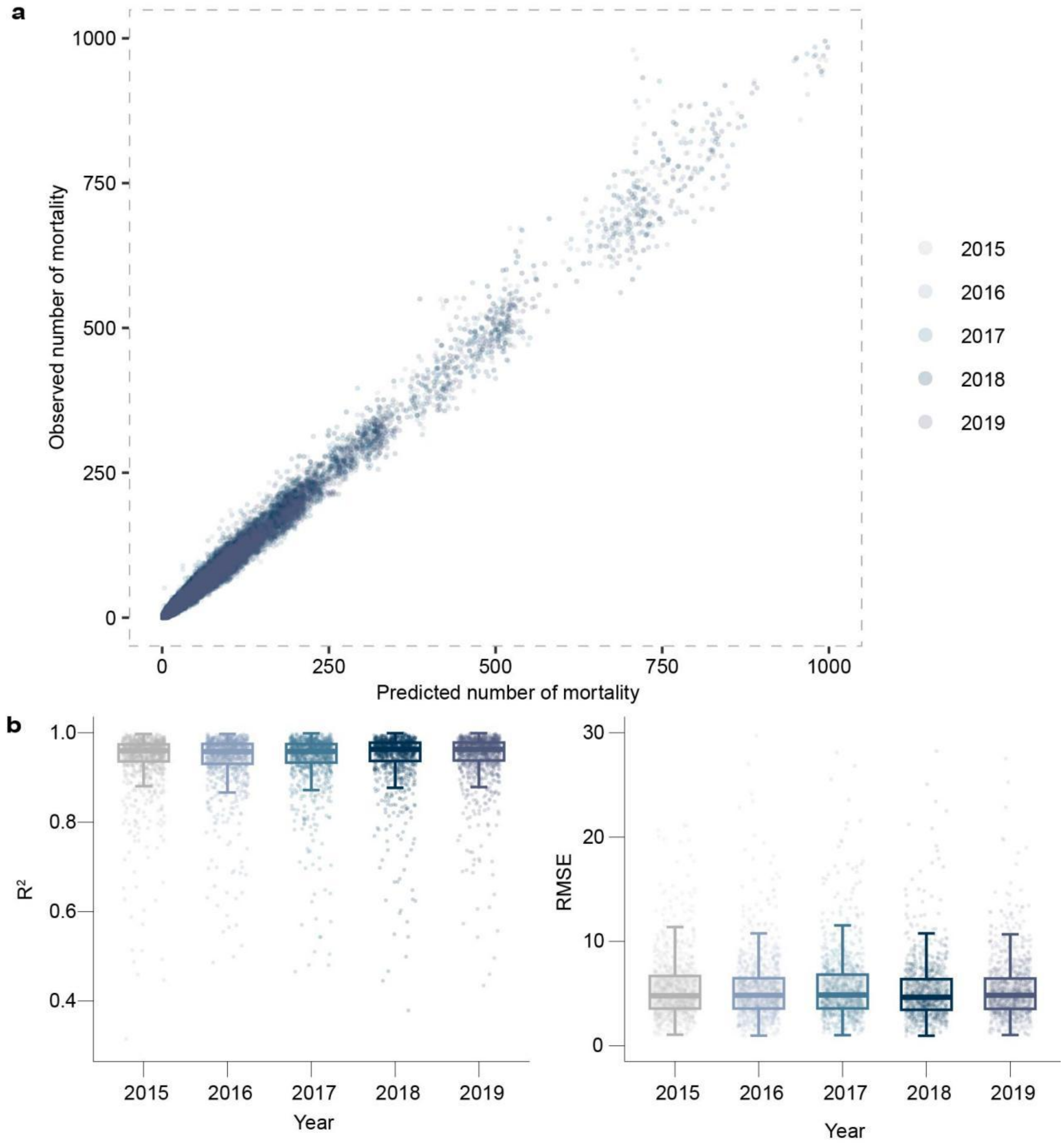

Supplementary Fig 5. The performance of the DLNM model based on leave-one-out cross validation. The scatterplot (a) compares the predicted number of deaths versus the observed number of deaths across 954 NUTS3-level regions. P-value is produced by two-sided Wilcoxon test. The boxplot (b) summarizes the R^2 and RMSE of the predicted number of deaths obtained from cross validation. The scatter in each box plot represents the point-to-point predictive accuracy.

C.3 Predictive accuracy validation

We further validated the predictive accuracy of the DLNM model with real-world observed data, as shown in Supplementary Fig 6. The results indicate a strong spatial correlation between observed and predicted mortality from June to August 2023. The adjusted R^2 for cumulative mortality reached 0.98, however, the RMSE estimated a deviation of 373 deaths under RCP4.5 and 359 deaths under RCP8.5 between observed and the predicted values. Worth noting is that our DLNM model was trained excluding data from 2020 onwards, when the global coronavirus disease 2019 (COVID-19) pandemic occurred. This means that our model cannot estimated the excess deaths caused by COVID-19. According to Our World in Data, Europe reported 390 cumulative deaths associated with COVID-19 during weeks 22-35, 2023. Despite the easing of various restrictions in many European countries from June to August 2023, the potential effect of coronavirus on excess mortality has not disappeared. Consequently, there may existed a fixed error between predicted and observed values, surpassing the predictive error of our model.

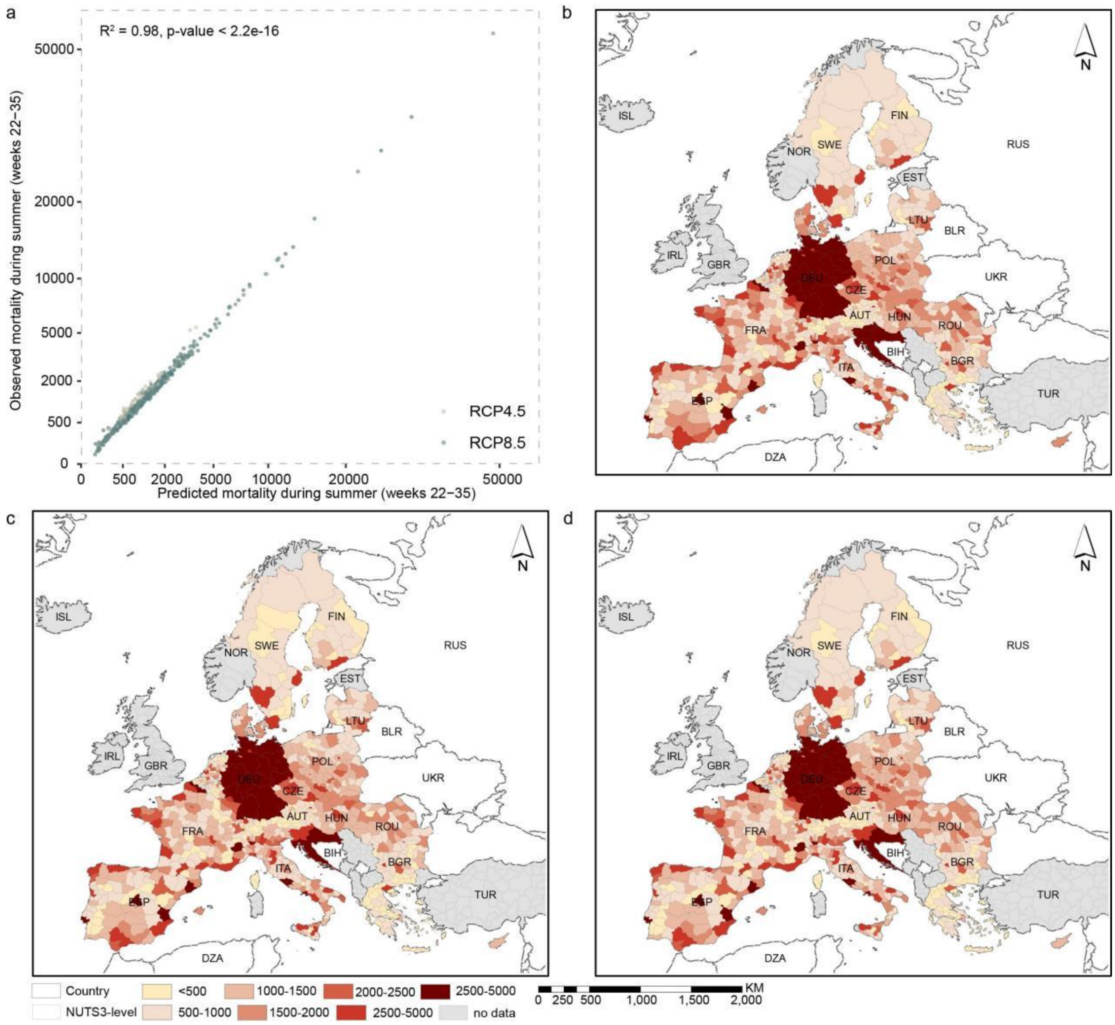

Supplementary Fig 6. The predictive accuracy of the DLNM model compared with the observed value of 2023. The scatterplot (a) compares the predicted number of deaths versus the observed number of deaths from June to August, 2023. P-value is produced by two-sided Wilcoxon test. The spatial observed (b), predicted number of deaths under RCP4.5(c) and RCP8.5(d) are categorized into 7 levels, ranging from light to dark: <500, 500-1000, 1000-1500, 1500-2000, 2500-5000 and >5000. Increasing shades of red indicate higher mortality in the regions.

C.4 Sensitivity analysis

To evaluate the robustness of our DLNM model, we designed several sensitivity analyses using various settings. The sensitivity analysis was aimed at investigating the impact of parameter settings on the relationship between heat-exposure and mortality. Specifically, we devised eight distinct scenarios (S1-S8 and DS) that varied the knots and the degrees of freedom in cross-basis function, as well as the degrees of freedom in natural cubic splines which used to control the long-term trends and seasonality. Additionally, we also replaced the functional forms of the exposure-response model and time-lag terms to test the responsiveness of the model to variations in the cross-basis function, as shown in scenarios SE1 and SE2.

- DS: The cross-basis function f was modeled using a natural spline function of degree 2 with one knot at 80th percentiles of weekly Humidex distribution and a time-lag effect function using a nature spline with integer lag values θ of 1, 2, and 4 weeks chosen by the log knots function. Two natural cubic splines of time with 4 degrees of freedom (df) for year number and 3 df for week number were employed to control the long-term trends and seasonality.
- SE1: The natural spline function was replaced with a B-spline function.
- SE2: The time-lag effect function was replaced by integer lag values up to 2 weeks (with minimum lag equal to 0 weeks by default).
- S1: The knot of B-spline was placed at the 70th percentiles of weekly Humidex distribution.

- S2: The knot of B-spline was placed at the 90^{th} percentiles of weekly Humidex distribution.
- S3: The degree of freedom of B-spline was set to 3.
- S4: The degree of freedom of B-spline was set to 4.
- S5: The degree of freedom for year number was set to 3.
- S6: The degree of freedom for year number was set to 5.
- S7: The degree of freedom for week number was set to 2.
- S8: The degree of freedom for week number was set to 5.

The results of our sensitivity analyses showed that the DLNM model was sensitive to the cross-basis functions (Supplementary Fig 7). Other parameters displayed negligible impact on the final results. Given these findings, we decided to set the degree of freedom of natural spline as 2 in our main analysis, as it yielded the narrowest confidence interval.

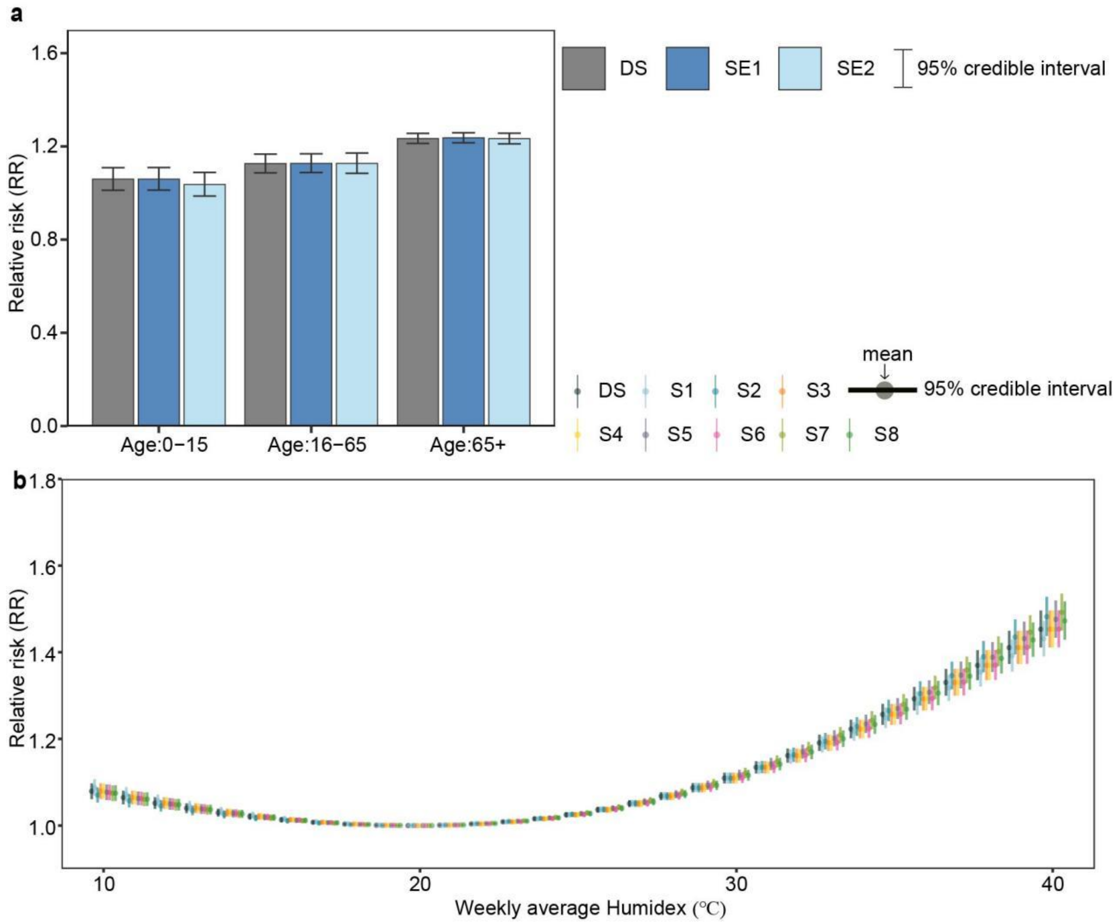

Supplementary Fig 7. Relative risk variation under different model settings via the cross-basis function (a) and other model terms (b).

D. Future heat-related mortality burden

D.1 Cumulative heat-related mortality burden from 2024 to 2080 at the NUTS3

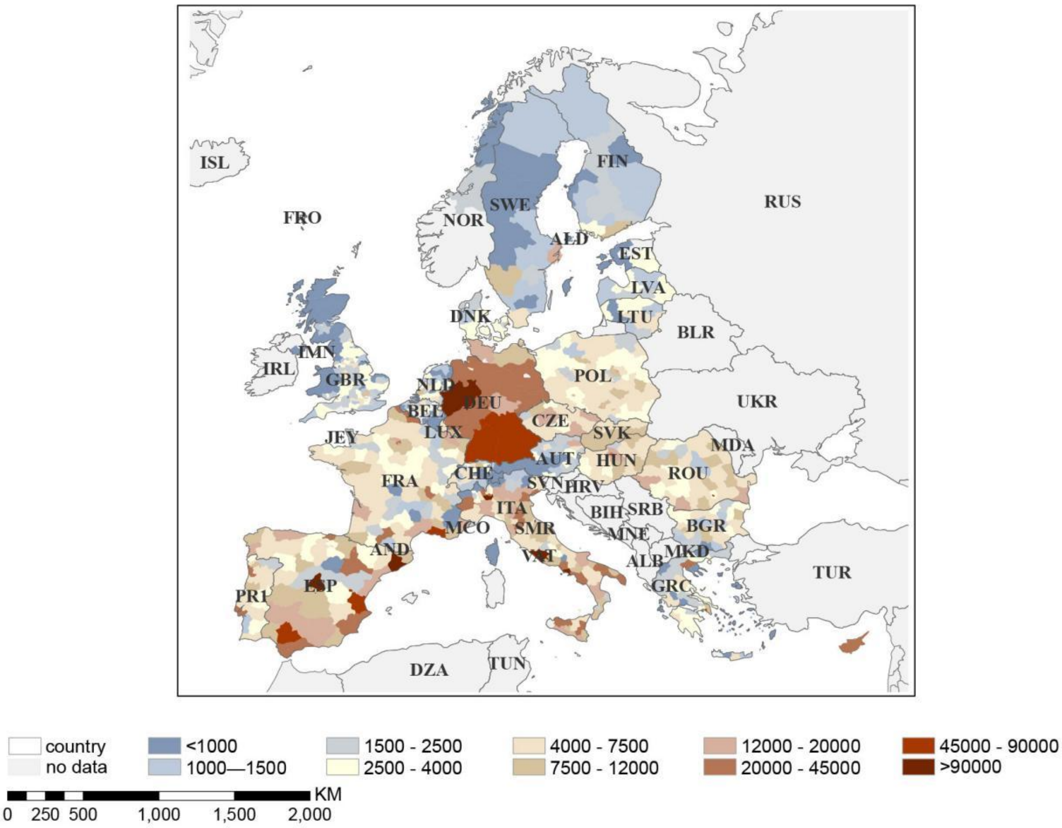

Supplementary Fig 8. Geographic pattern of cumulative heat-related mortality burden from 2024 to 2080 at the NUTS3 level under RCP4.5-SSP1. The regions with missing data are shaded in gray. The cumulative heat-related mortality burden indicates the predicted total number of deaths associated with extreme heat during 2024 to 2080.

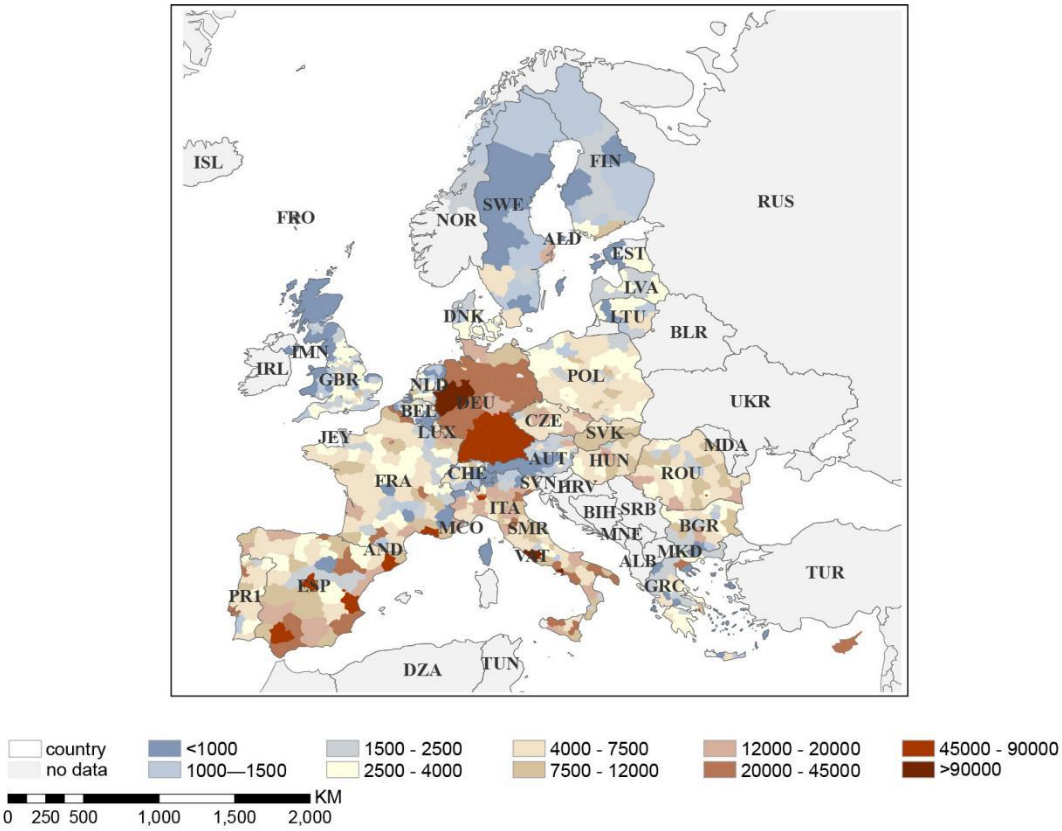

Supplementary Fig 9. Geographic pattern of cumulative heat-related mortality burden from 2024 to 2080 at the NUTS3 level under RCP4.5-SSP2. The regions with missing data are shaded in gray. The cumulative heat-related mortality burden indicates the predicted total number of deaths associated with extreme heat during 2024 to 2080.

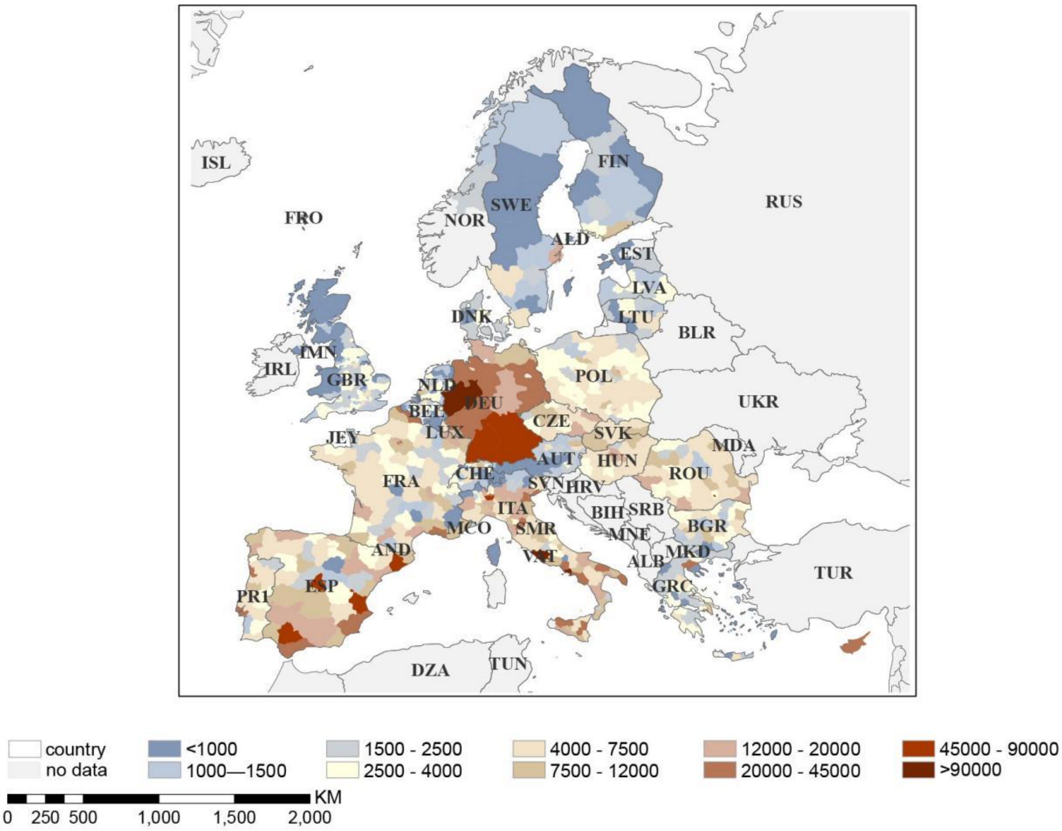

Supplementary Fig 10. Geographic pattern of cumulative heat-related mortality burden from 2024 to 2080 at the NUTS3 level under RCP4.5-SSP4. The regions with missing data are shaded in gray. The cumulative heat-related mortality burden indicates the predicted total number of deaths associated with extreme heat during 2024 to 2080.

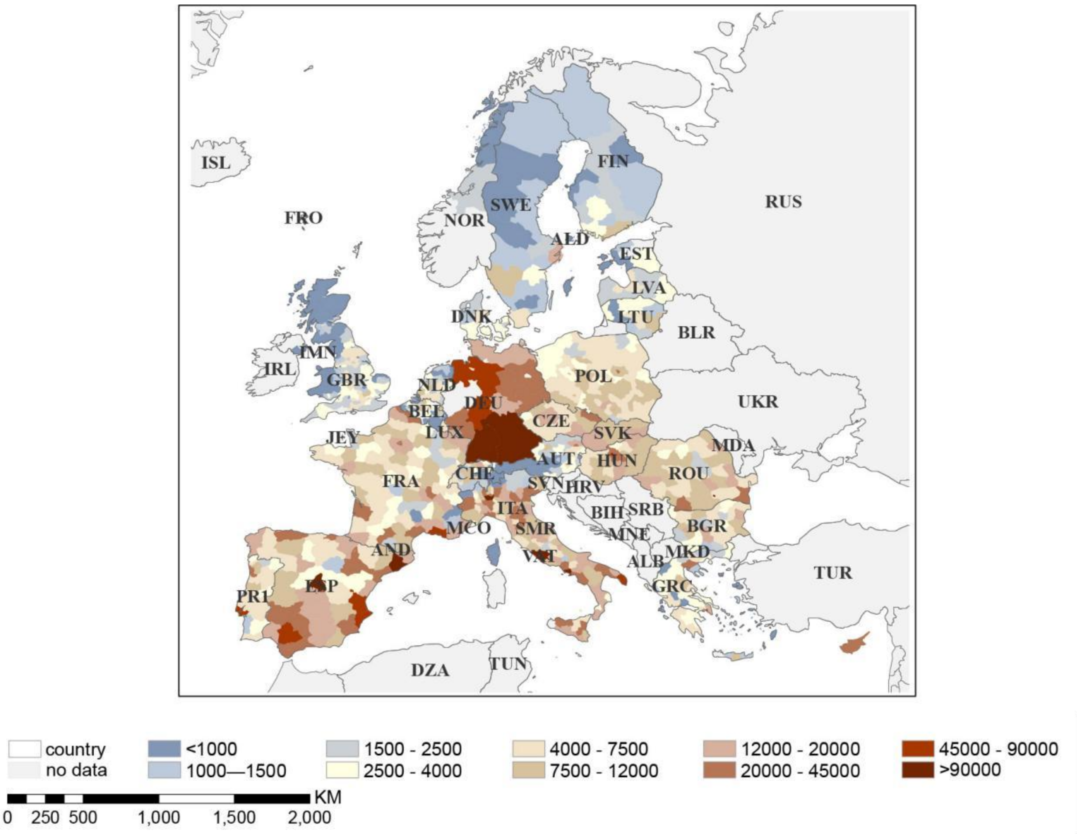

Supplementary Fig 11. Geographic pattern of cumulative heat-related mortality burden from 2024 to 2080 at the NUTS3 level under RCP8.5-SSP1. The regions with missing data are shaded in gray. The cumulative heat-related mortality burden indicates the predicted total number of deaths associated with extreme heat during 2024 to 2080.

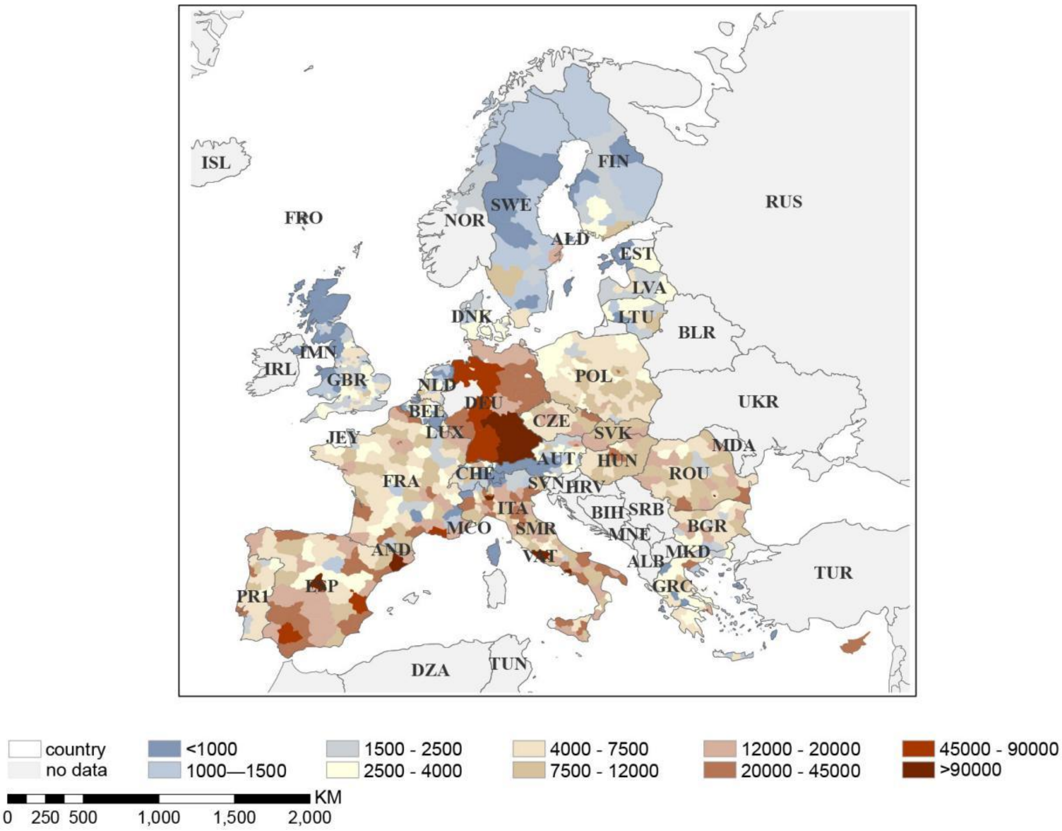

Supplementary Fig 12. Geographic pattern of cumulative heat-related mortality burden from 2024 to 2080 at the NUTS3 level under RCP8.5-SSP2. The regions with missing data are shaded in gray. The cumulative heat-related mortality burden indicates the predicted total number of deaths associated with extreme heat during 2024 to 2080.

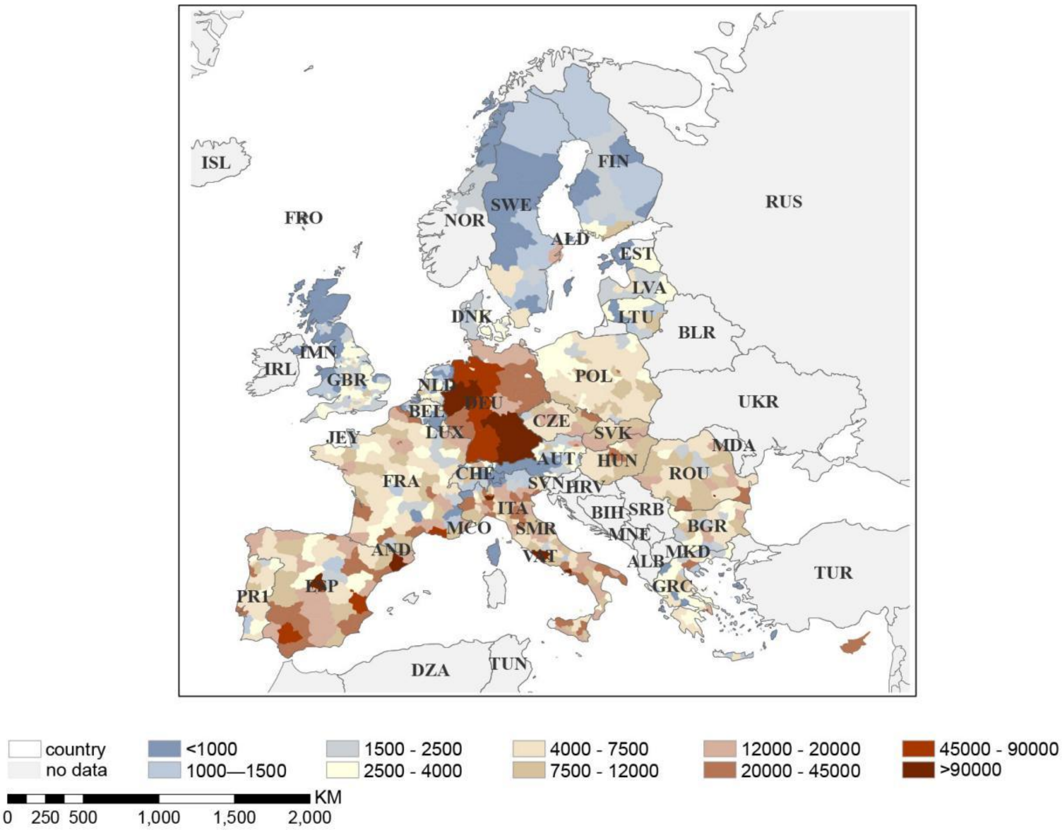

Supplementary Fig 13. Geographic pattern of cumulative heat-related mortality burden from 2024 to 2080 at the NUTS3 level under RCP8.5-SSP4. The regions with missing data are shaded in gray. The cumulative heat-related mortality burden indicates the predicted total number of deaths associated with extreme heat during 2024 to 2080.

E. Roles of climate change, population growth and aging

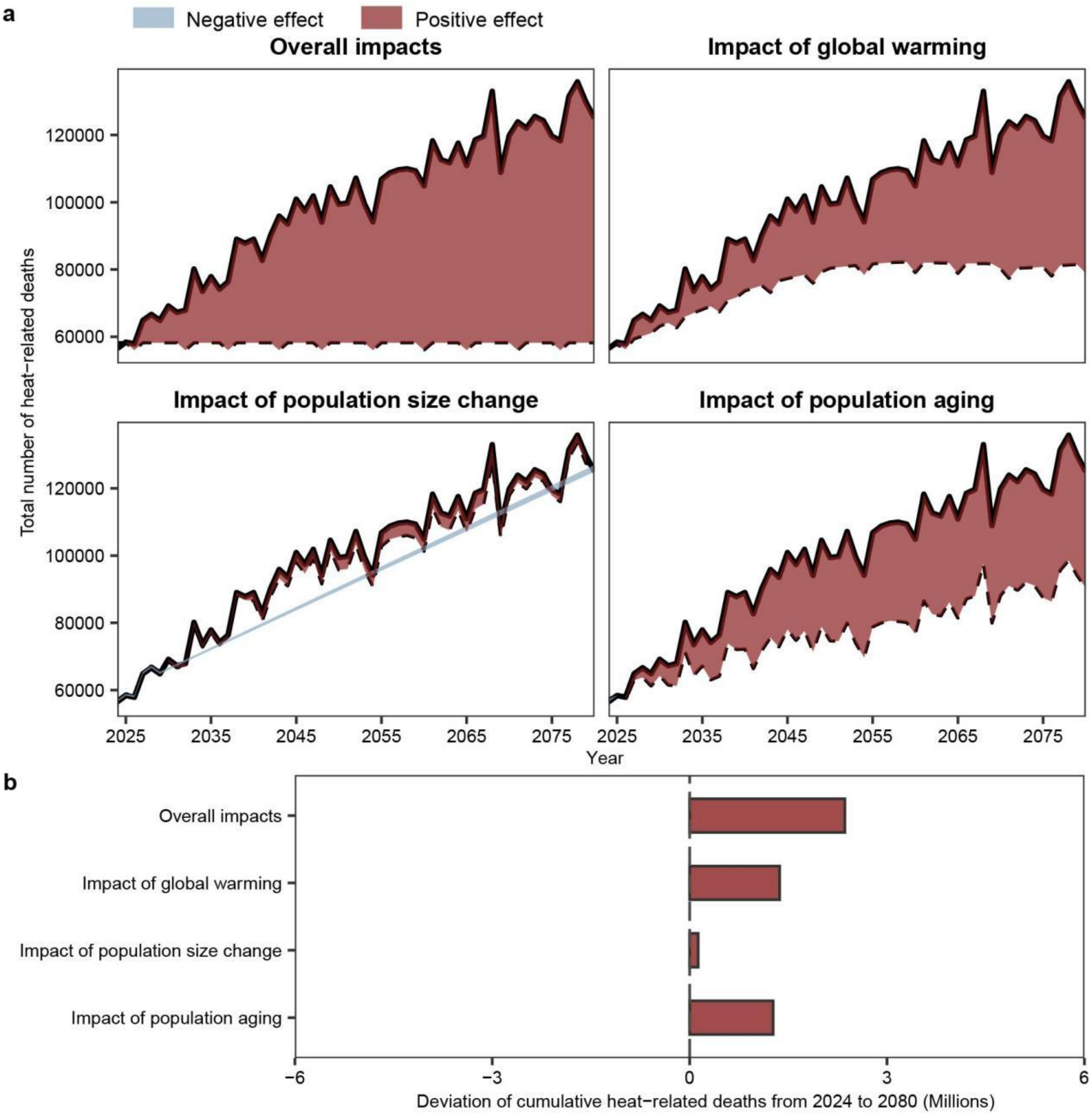

Supplementary Fig 14. Decomposition analysis of driving factors of future heat-related death growth in Europe under RCP4.5-SSP1.

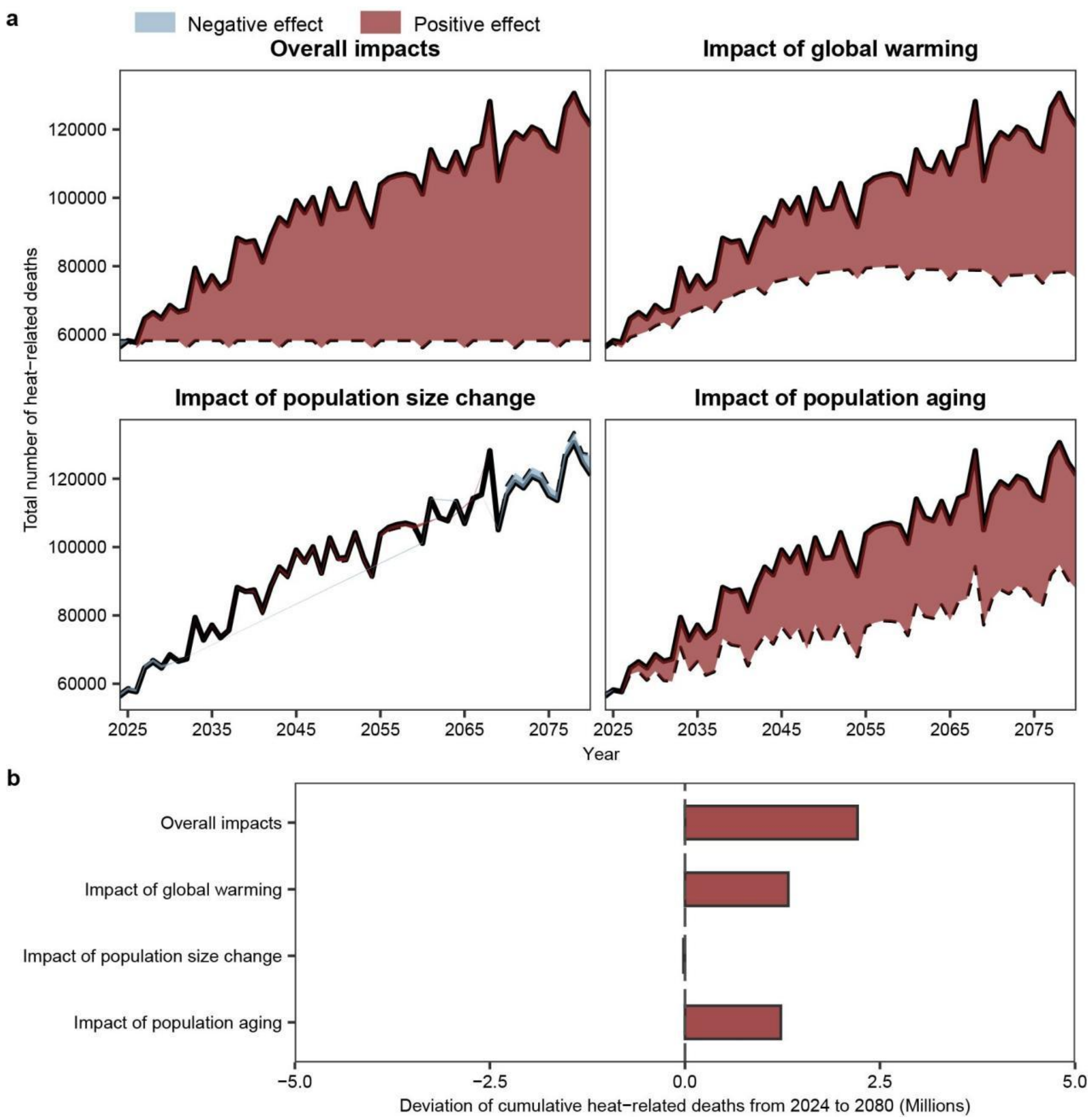

Supplementary Fig 15. Decomposition analysis of driving factors of future heat-related death growth in Europe under RCP4.5-SSP2.

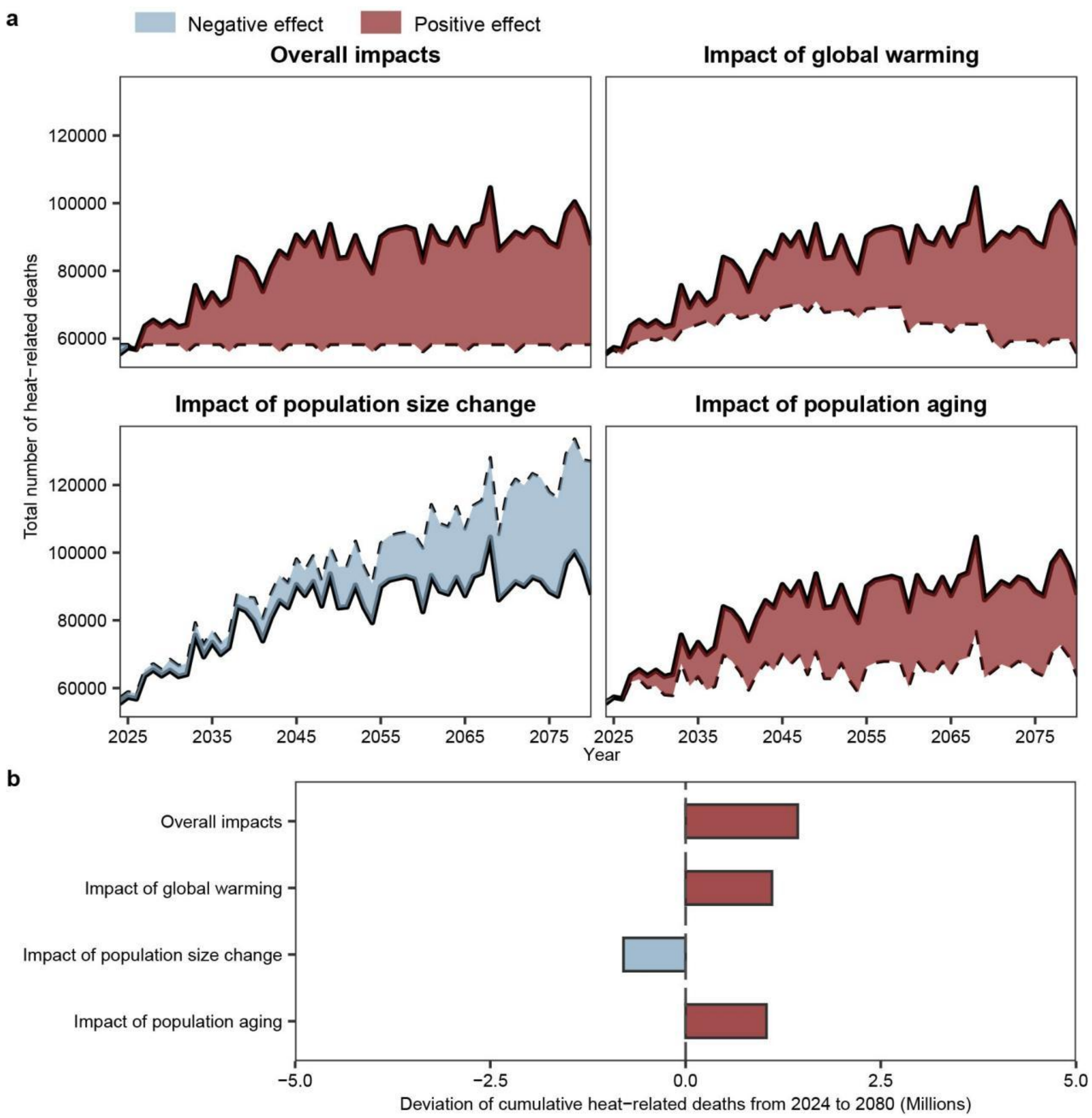

Supplementary Fig 16. Decomposition analysis of driving factors of future heat-related death growth in Europe under RCP4.5-SSP3.

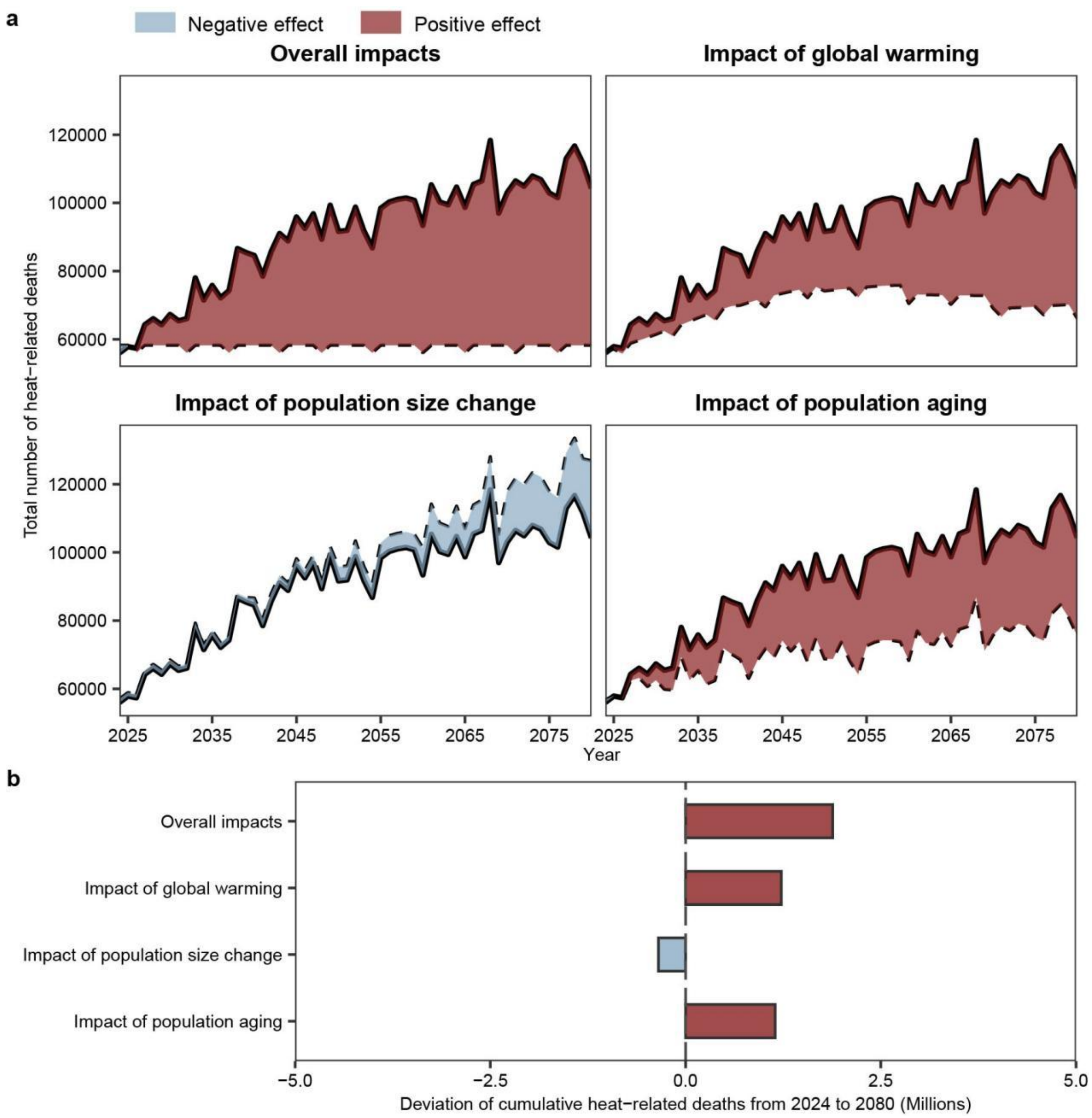

Supplementary Fig 17. Decomposition analysis of driving factors of future heat-related death growth in Europe under RCP4.5-SSP4.

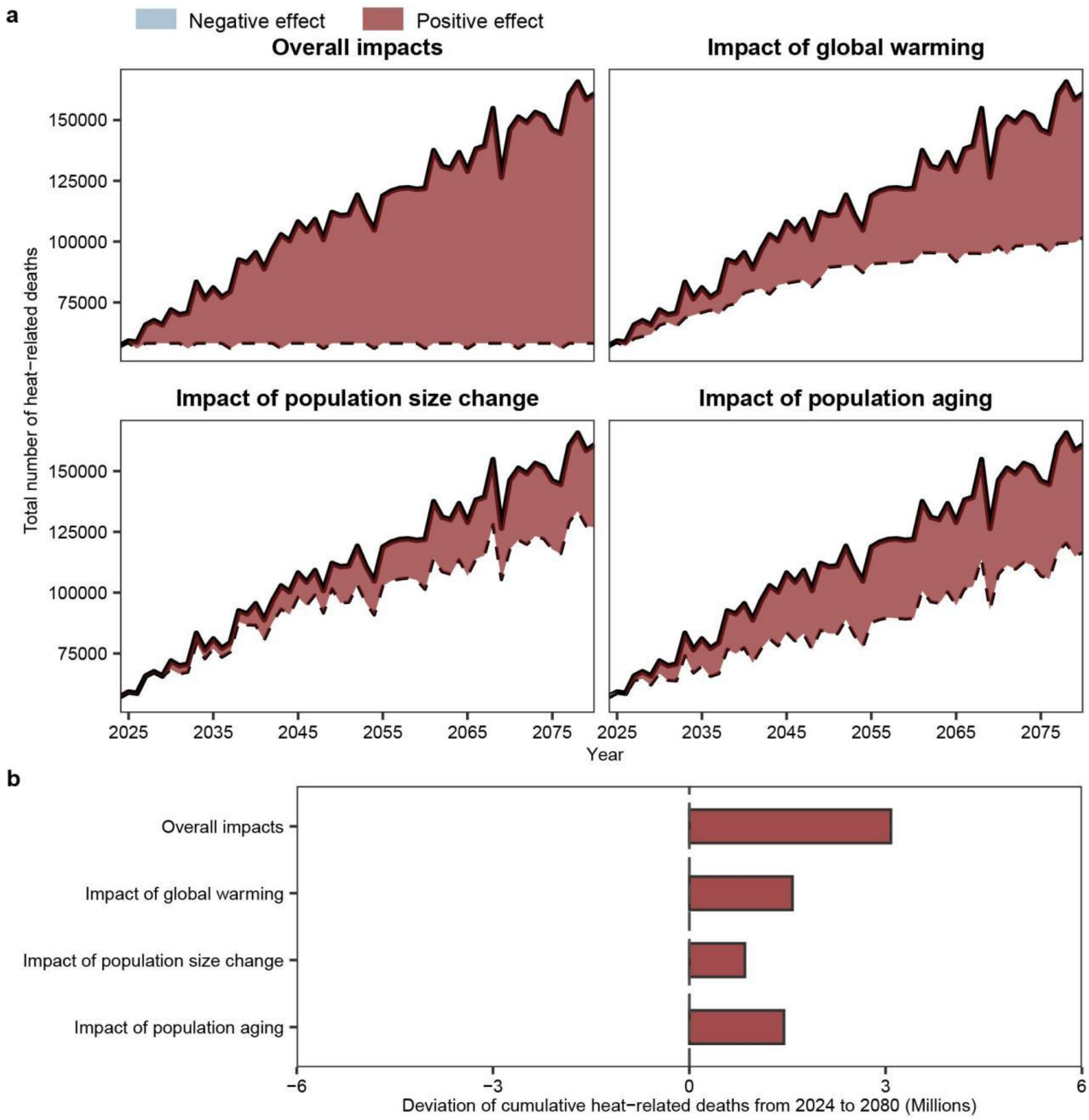

Supplementary Fig 18. Decomposition analysis of driving factors of future heat-related death growth in Europe under RCP4.5-SSP5.

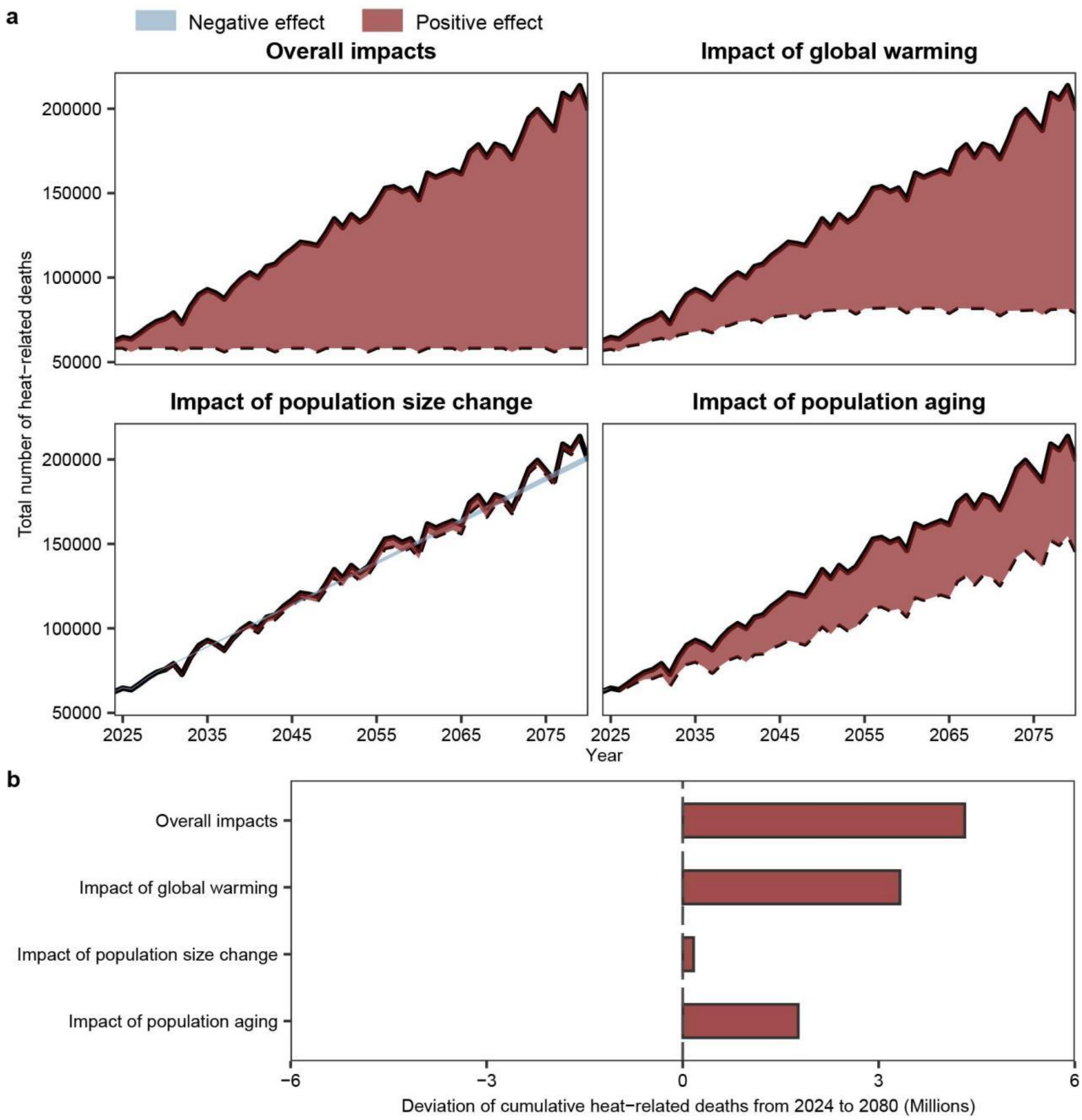

Supplementary Fig 19. Decomposition analysis of driving factors of future heat-related death growth in Europe under RCP8.5-SSP1.

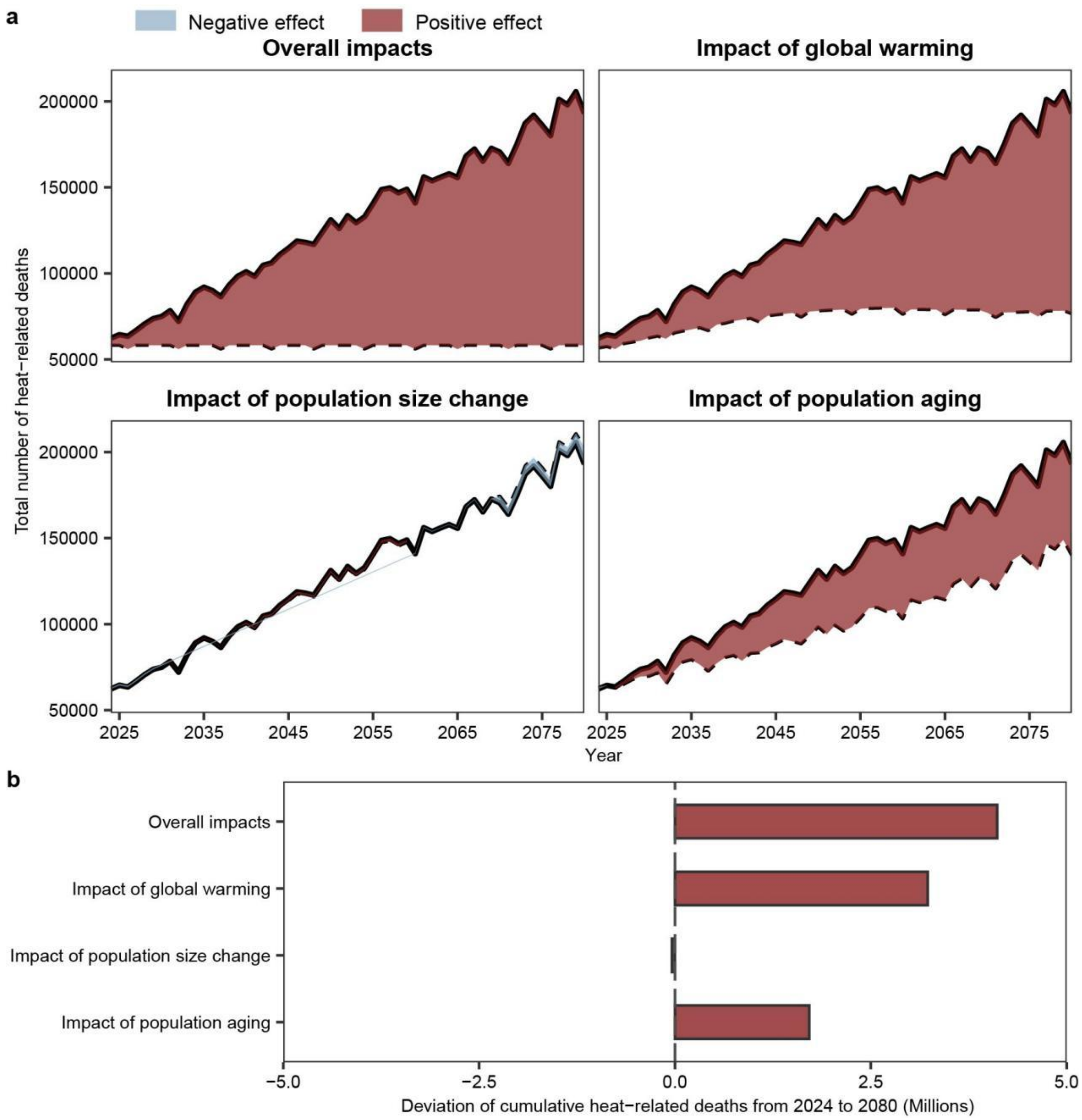

Supplementary Fig 20. Decomposition analysis of driving factors of future heat-related death growth in Europe under RCP8.5-SSP2.

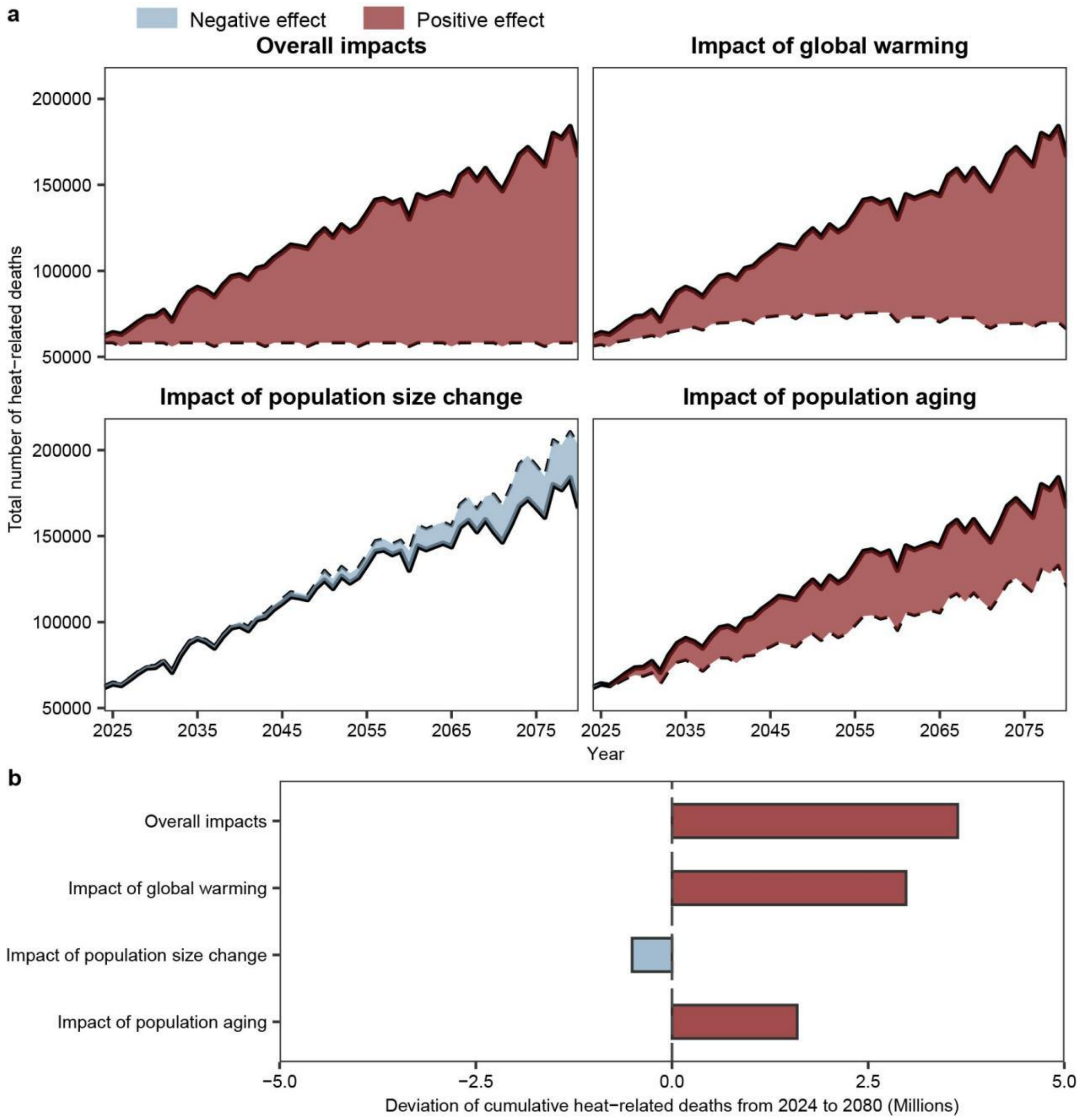

Supplementary Fig 21. Decomposition analysis of driving factors of future heat-related death growth in Europe under RCP8.5-SSP4.

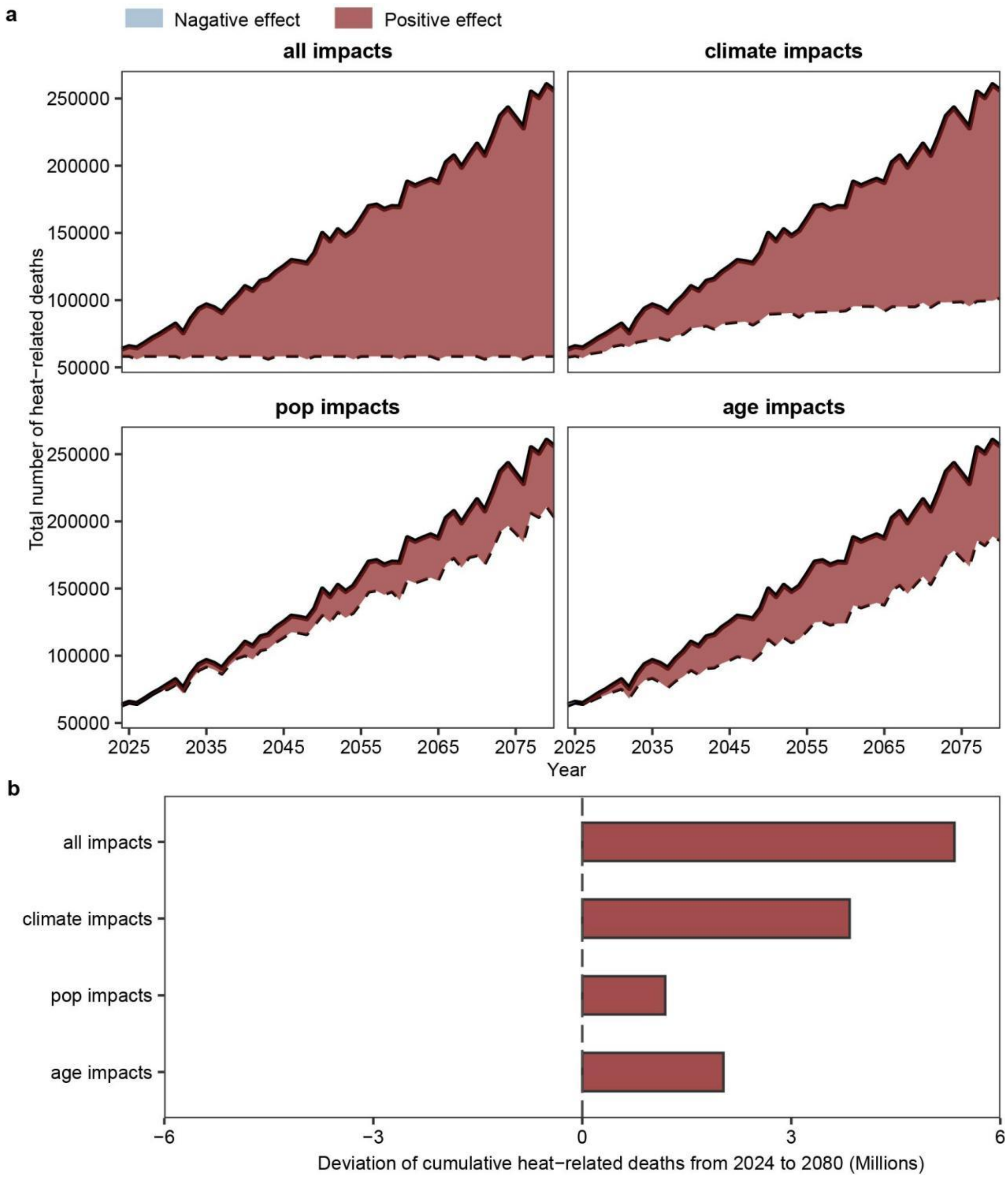

Supplementary Fig 22. Decomposition analysis of driving factors of future heat-related death growth in Europe under RCP8.5-SSP5.

Reference

1. McCuen, R. H., Knight, Z. & Cutter, A. G. Evaluation of the Nash–Sutcliffe Efficiency Index. *J Hydrol Eng* **11**, 597–602 (2006).